ELSEVIER

COMPTES RENDUS

MECANIQUE

Instabilities and bifurcations due to buoyancy in a cylindrical container heated from below with and without a free surface

Anas El Gallaf [a,*], Ridha Touihri [b], Daniel Henry [a], Hamda Ben Hadid [a]

[a] *Laboratoire de mécanique des fluides et d'acoustique, CNRS/Université de Lyon, École centrale de Lyon/Université Lyon 1/INSA de Lyon, ECL, 36, avenue Guy-de-Collongue, 69134 Ecully cedex, France*
[b] *LAMSIN, ENIT, campus universitaire, le belvédère, BP 37, 1002 Tunis, Tunisie*

Abstract

Three-dimensional simulations of the buoyant convection in a cylindrical container heated from below are presented. Both the thresholds for the onset of the convection and the nonlinear evolution of this convection are calculated. The simulations concern two configurations: a cavity with a rigid upper surface (Rigid-Rigid case) and a cavity with a non-constrained free surface (Rigid-Free case). The results show a similar variation of the primary thresholds with the aspect ratio for the two configurations. In contrast, the nonlinear evolution of the convection is much changed between the two configurations. In particular, subcritical secondary branches with a very large subcriticity are obtained in the R-F case. *To cite this article: A. El Gallaf et al., C. R. Mecanique 337 (2009).*

© 2009 Académie des sciences. Published by Elsevier Masson SAS. All rights reserved.

1. Introduction

Convection arising in a layer heated from below is a classical problem in fluid mechanics. This problem has more recently induced new research activities to take into account finite-size containers, particularly cylindrical containers. When the layer is confined between two rigid upper and lower boundaries, the flow is buoyancy driven and the governing parameter is the well-known Rayleigh number. For a comprehensive introduction and a bibliographical review of the buoyancy driven instability in closed cylindrical containers, we refer to the work of Touihri et al. [1] and the references therein. The dynamics and the bifurcation scenarios become more complicated in the presence of an upper free surface, especially since there is a geometry related inhomogeneity. The flow patterns observed above the critical thresholds are strongly influenced by the absence of reflection symmetry in the mid-plane of the container. A consequence is the prevalence of hexagonal structures in extended domains. In comparison to the closed container

---

* Corresponding author.

E-mail addresses: anas.el-gallaf@ec-lyon.fr (A. El Gallaf), ridha.touihri@ipeim.rnu.tn (R. Touihri), daniel.henry@ec-lyon.fr (D. Henry), hamda.benhadid@univ-lyon1.fr (H. Ben Hadid).

(Rigid-Rigid case), the presence of an upper free surface (Rigid-Free case) also allows the development of an extra driving mechanism due to the surface tensions. This mechanism is denoted as the Marangoni effect and its influence is quantified by the Marangoni number. The respective influence of gravity and capillarity on the onset of convective flows largely depends on the thickness of the layer (height of the container). For a fixed container radius, this dependence is observed with respect to the aspect ratio A (= radius/height) of the container. In small aspect ratio boxes, the flow is mainly gravity driven while the Marangoni effect is dominant for flattened boxes. In boxes of intermediate sizes, both effects can be effective and the problem is known as the Marangoni–Bénard problem. The reference experimental work on the Marangoni–Bénard instability in circular containers has been performed by Koschmieder and Prahl [2]. More recent works have measured the free surface deformation associated with the flow pattern [3,4]. Linear stability studies on the Marangoni–Bénard problem have taken into account the simultaneous variation of the Marangoni and Rayleigh numbers when the applied vertical temperature difference is progressively increased (Zaman and Narayanan [5], Dauby et al. [6]). They verified that for small aspect ratios buoyancy is dominant while for large aspect ratios Marangoni effect is dominant. They made comparisons with the experiments of Koschmieder and Prahl [2] and found critical values 20% higher than in the experiments. The three-dimensional studies about the nonlinear evolution of the convection in cylindrical containers are few. We can mention the recent work of Assemat et al. [7] in the case of the pure Marangoni convection.

Our work is devoted to the buoyancy driven convection in cylindrical containers. We want to see the influence played by the dynamical condition at the upper boundary. For that, both R-R situations with a solid upper surface (no-slip condition) and R-F situations with a non-constrained free surface are considered. In both cases, the temperature at the upper surface will be considered as nearly uniform, either fixed or resulting from a high Bi number. Three-dimensional simulations using continuation techniques will be performed which will allow to calculate both the thresholds for the onset of convection and the nonlinear evolution of the emerging convective flows. The governing equations and the numerical techniques will be briefly described in the next section. Results will be presented in Section 3 and a conclusion summarizing the main observations will then be given.

2. Governing equations

We consider an incompressible fluid layer confined in a cylinder between two (Rigid-Rigid case) or one (Rigid-Free case) perfectly heat-conducting horizontal circular plates and a lateral adiabatic side wall. The cylinder of aspect ratio $A = R/H$ is exposed to a vertical gravitation acceleration g and to a vertical temperature gradient $\Delta T/H = (T_b - T_t)/H$ directed from bottom to top. T_b and T_t are the bottom and top temperatures in the diffusive regime, respectively, H is the layer thickness (or cylinder height) and R the cylinder radius. The fluid is assumed to be Newtonian with constant physical properties, except that the fluid density ρ depends linearly on temperature in the buoyancy term.

For the R-F case, a Newton law of cooling, $-\lambda \partial_z T = h(T - T_g)$, expresses the heat transfer between the free surface and the ambient gas at constant temperature T_g (λ is the liquid thermal conductivity, and h is the heat exchange coefficient). As a consequence, $T_t = [-Bi(T_b - T_g)/(1 + Bi)] + T_b$, where $Bi = hH/\lambda$ is the Biot number. Moreover, the upper surface is assumed to be flat and free of surface tension.

The convective flow is governed by the incompressible Navier–Stokes equations coupled to an energy equation. Using H, H^2/ν, ν/H and ΔT (ν is the kinematic viscosity) as scales for length, time, velocity and temperature (the dimensionless temperature is $\theta = (T - T_t)/\Delta T$), these equations take the following form:

$$\nabla \cdot \boldsymbol{u} = 0 \tag{1}$$

$$\frac{\partial \boldsymbol{u}}{\partial t} + (\boldsymbol{u} \cdot \nabla)\boldsymbol{u} = -\nabla p + \nabla^2 \boldsymbol{u} + Ra\,Pr^{-1}\theta\boldsymbol{e}_z \tag{2}$$

$$\frac{\partial \theta}{\partial t} + (\boldsymbol{u} \cdot \nabla)\theta = Pr^{-1}\nabla^2\theta \tag{3}$$

where $Pr = \nu/\kappa$ is the Prandtl number and $Ra = \beta g \Delta T H^3/(\nu\kappa)$ is the Rayleigh number (κ is the thermal diffusivity and β the thermal expansion coefficient). Knowing that no-slip boundary conditions are applied at the rigid walls, the boundary conditions are given by

$$\boldsymbol{u} = 0 \quad \text{and} \quad \frac{\partial \theta}{\partial r} = 0 \quad \text{at } r = A \tag{4}$$

$$\boldsymbol{u} = 0 \quad \text{and} \quad \theta = 1 \quad \text{at } z = 0 \tag{5}$$

$$\boldsymbol{u} = 0 \quad \text{and} \quad \theta = 0 \quad \text{at } z = 1 \quad \text{(R-R)} \tag{6}$$

$$\frac{\partial u}{\partial z} = \frac{\partial v}{\partial z} = w = 0 \quad \text{and} \quad \frac{\partial \theta}{\partial z} + Bi\,\theta + 1 = 0 \quad \text{at } z = 1 \quad \text{(R-F)} \tag{7}$$

The conductive rest state solution corresponds to a linear temperature profile along the vertical coordinate which, in dimensionless form, is given by $\theta(z) = 1 - z$.

In the three-dimensional cylindrical cavity, the governing equations are solved using a spectral element method [1]. The time discretization is carried out using a semi-implicit splitting scheme and a continuation technique based on a Newton solver is implemented, which allows both steady state solving and direct calculation of the bifurcation points as described in Henry and Ben Hadid [8]. The primary bifurcation points at which convection is triggered need first to be calculated. Due to the symmetries of the problem which include those of the $\mathcal{O}(2)$ symmetry group, the modes which are involved are Fourier modes with an azimuthal variation expressed as $\exp(im\varphi)$ (principally the $m = 0$, 1 and 2 modes). Then the steady solutions branches which emerge at these bifurcation points can be followed by continuation and bifurcation diagrams showing how these solutions evolve and are connected can be plotted.

3. Results

3.1. Accuracy and precision

After mesh refinement tests, a mesh with $(N_{xy} \times N_z) = (320 \times 10)$ points has been chosen for all calculations, where N_{xy} represents the number of points in the circular section of the cylinder and N_z the number of points in the vertical direction. This mesh enables a precise computation of the critical thresholds for the whole range of parameters considered (accuracy estimated at 0.1%). A good agreement was found between our results and those given by previous authors (Touihri et al. [1] for the R-R case and Dauby et al. [6] for the R-F case). As an example, Touihri et al. estimated a first transition at $Ra_c = 2260.13$ for R-R cavities with $A = 1$ and our code gives $Ra_c = 2260.06$. For R-F cavities with $Bi = 1$, Dauby et al. found a critical value $Ra_c = 1628.20$ for an aspect ratio $A = 1$ to be compared with our $Ra_c = 1628.11$.

3.2. Thresholds for the onset of convection

The thresholds Ra_c for the onset of convection (which are independent of Pr) are given in Fig. 1 as a function of the aspect ratio A for the R-R case (Fig. 1(a)) and the R-F case for $Bi = 100$ (good approximation for a thermally conducting upper boundary) (Fig. 1(b)). Only the lowest thresholds corresponding to the first three Fourier modes are plotted, and the true critical threshold at which a stable convective flow is first triggered is given by the lowest value. For both R-R and R-F cases, there is a clear stabilization effect induced on the thresholds by the confinement. The evolution of the critical threshold is also not regular because, depending on the aspect ratio, different modes are involved. For the small values of A (narrow cylinders with A roughly below 1), a one-roll $m = 1$ mode is involved at the critical threshold, whereas for larger A (flat cylinders for which the lateral constraint is weaker) different modes are successively involved, first the axisymmetric $m = 0$ mode and then again the $m = 1$ mode. In fact, for small values of A, the lateral confinement constrains the convective structures (only a limited number of convective rolls can be formed). This explains that the convective one roll $m = 1$ mode is dominant for cells having very small values of A. For larger A, it is the axisymmetric (two-roll) $m = 0$ mode which is then preferred, before the $m = 1$ mode becomes again dominant. This $m = 1$ mode has in fact evolved with the increase of A and is now a three-roll structure. The evolution from one roll to three rolls by the simultaneous creation of two small rolls along the boundaries is initiated in the range $1.1 < A < 1.3$ where changes of curvatures are observed in the critical curves for this mode. This evolution also keeps all the symmetries of the $m = 1$ mode. Finally, for large values of A, the critical modes have closer thresholds as the modes can easily adapt themselves to the geometry by adding extra rolls near the end walls.

If the evolution of the thresholds looks similar in the R-R and R-F cases, a more detailed comparison between the two cases show that the values of A at which the transitions between the modes occur are slightly larger for the R-F case: the first transition from $m = 1$ to $m = 0$ is changed from $A \approx 0.91$ for the R-R case to $A \approx 1.03$ for the R-F case, and the second transition from $m = 0$ to $m = 1$ is changed from $A \approx 1.57$ to $A \approx 1.85$. Moreover, the values of the
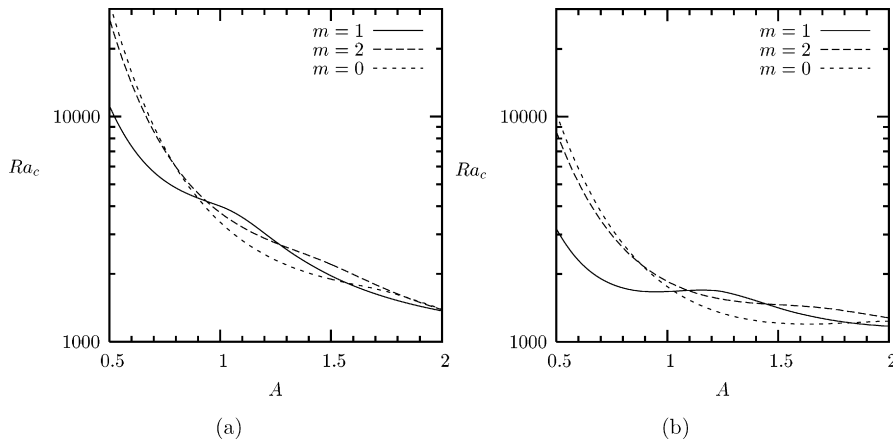
Fig. 1. Evolution of the primary thresholds Ra_c for the onset of buoyancy induced convection in a cylindrical container as a function of the aspect ratio A. The three main convective modes (Fourier modes $m = 0$, 1 and 2) are considered. The results are shown for (a) the R-R case (solid upper boundary) and (b) the R-F case (non-constrained free upper boundary).

thresholds are larger in the R-R case than in the R-F case ($Ra_c = 11\,191$ compared to $Ra_c = 3212$ and $Ra_c = 1371$ compared to $Ra_c = 1185$ for $A = 0.5$ and 2, respectively) which indicates a stabilization induced by the upper rigid boundary, this stabilization being particularly strong for small aspect ratio cylinders. Finally, the differences in the boundary conditions between the R-R and R-F cases create differences in the symmetries: a reflection symmetry with respect to the horizontal mid-plane is effective in the R-R case, but does not exist in the R-F case. This will affect the nature of the first bifurcations: in the R-R case, this reflection symmetry is broken at the onset of convection so that all these bifurcations are pitchforks whereas in the R-F case, only the bifurcations associated with non-axisymmetric modes ($m \geqslant 1$) are pitchforks as the bifurcation associated with the axisymmetric mode does not break any symmetry and is then transcritical. In the next section, we will see how differently the primary axisymmetric flows will evolve in the two R-R and R-F cases.

3.3. Nonlinear evolution of the convection

The nonlinear evolution of the steady convective regimes initiated at the primary thresholds is depicted through bifurcation diagrams. These diagrams show the vertical velocity w_0 at the center of the cavity as a function of the Rayleigh number Ra. Stable regimes are plotted as solid lines and unstable regimes as dashed lines. With the choice of w_0, the bifurcations associated to the axisymmetric mode appear symmetric when they are pitchforks (the solutions on one branch are obtained from those on the other by reflexion in z) and they appear non-symmetric when they are transcritical. In the former case, we therefore only need to present the evolution of one of the two branches. In the diagrams, the flows on the different branches are also depicted through plots of the vertical velocity w at mid-height, with dark (light) shading indicating $w < 0$ ($w > 0$). The calculations have been done for $Pr = 1$.

The bifurcation diagram given in Fig. 2 has been obtained in the R-R case for an aspect ratio $A = 1$. As shown in Fig. 1(a), for this aspect ratio convection is initiated by an axisymmetric $m = 0$ mode at $Ra_c = 2260$. The bifurcation is a supercritical pitchfork and the two branches of dynamically equivalent axisymmetric solutions remain stable until a secondary bifurcation point located at $Ra_S = 3003$. The destabilization at this point is associated with critical $m = 2$ modes and the supercritically emerging branches correspond to solutions defined to within a rotation around the cylinder axis (circular pitchfork bifurcation). These $m = 0/2$ solutions (combination of the axisymmetric $m = 0$ solution and $m = 2$ modes) consist of two counter-rotating and parallel rolls which preserve two symmetries, i.e. the reflection symmetries with respect to the two vertical central planes either parallel or perpendicular to the roll axes. The $m = 0/2$ branches are stable up to another steady bifurcation point. Another bifurcation diagram was obtained for a cylinder of aspect ratio $A = 1.5$. This bifurcation diagram is simpler as the primary axisymmetric flow initiated at a pitchfork bifurcation point at $Ra_c = 1895$ remains stable in the range of studied Rayleigh numbers ($Ra < 20\,000$).

The bifurcation diagram in the R-F case for an aspect ratio $A = 1.5$ and a Biot number $Bi = 100$ is shown in Fig. 3. This bifurcation diagram looks very different from those obtained in the R-R case. The conduction state is stable up
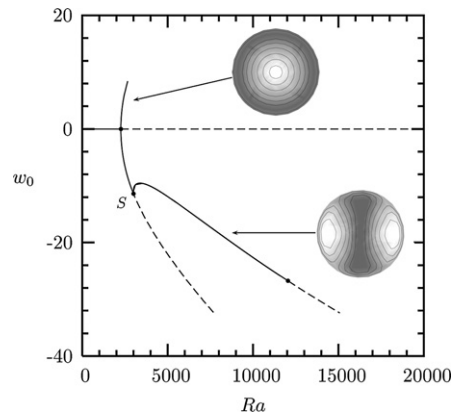
Fig. 2. Bifurcation diagram for the buoyancy induced convection developing in a cylinder with a solid upper boundary (R-R case) and an aspect ratio $A = 1$ ($Pr = 1$). Continuous lines indicate stable states and dashed lines unstable states. Black dots indicate steady bifurcation points and circles Hopf bifurcation points. Insets show vertical velocity contours in the horizontal mid-plane of the cylinder.
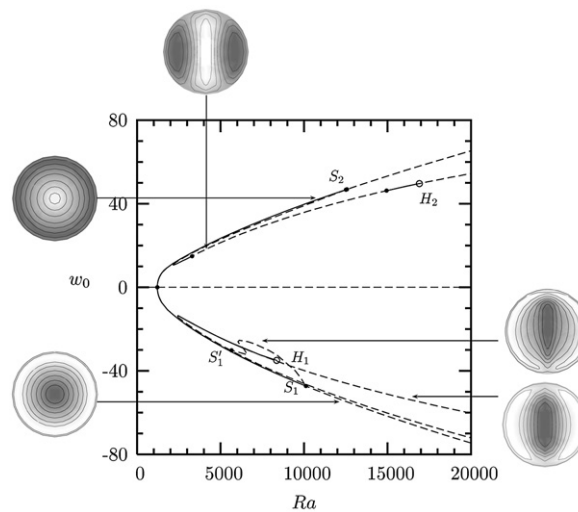
Fig. 3. Bifurcation diagram for the buoyancy induced convection developing in a cylinder with a non-constrained free upper boundary (R-F case) and an aspect ratio $A = 1.5$ ($Pr = 1$). Continuous lines indicate stable states and dashed lines unstable states. Black dots indicate steady bifurcation points and circles Hopf bifurcation points. Insets show vertical velocity contours in the horizontal mid-plane of the cylinder.

to $Ra_c = 1212$ where it is now a transcritical bifurcation which is associated to the onset of the axisymmetric flow. Two branches of axisymmetric solutions emerge, the upper one which is also represented in Fig. 4(a) being subcritical (the subcriticality is so weak that it cannot be seen on the figure) and the lower one which can be seen more clearly in Fig. 4(b) supercritical. On the upper branch (up-flow along the axis of the cylinder), the flow remains stable up to $Ra_{S_2} = 12\,512$ where critical $m = 2$ eigenmodes generate a circle of $m = 0/2$ solutions. These branches, however, bifurcate subcritically so that the solutions are unstable until a saddle-node bifurcation at $Ra = 2154$ where they are stabilized. The branches are further destabilized by a steady mode in the range $3292 < Ra < 14\,948$ before they reach a Hopf bifurcation point at $Ra_{H_2} = 16\,908$. On the lower branch (down-flow in the center of the cavity), the scenario to reach the $m = 0/2$ solutions is still more complex. The axisymmetric flow remains stable up to $Ra_{S_1} = 10\,112$, but the destabilization is now associated to $m = 1$ eigenmodes. The circle of $m = 0/1$ solutions (with only one vertical plane of symmetry) bifurcate subcritically and are then unstable. Such branches remain unstable and after different saddle-node bifurcations they terminate at a bifurcation point at $Ra_{S_1'} = 5656$ where they reach branches of unstable $m = 0/2$ solutions. The $m = 0/2$ solutions remain unstable for increasing Ra. For decreasing Ra, they are eventually stabilized at a saddle-node bifurcation at $Ra = 2382$, before they reach a Hopf bifurcation point at $Ra_{H_1} = 8361$.
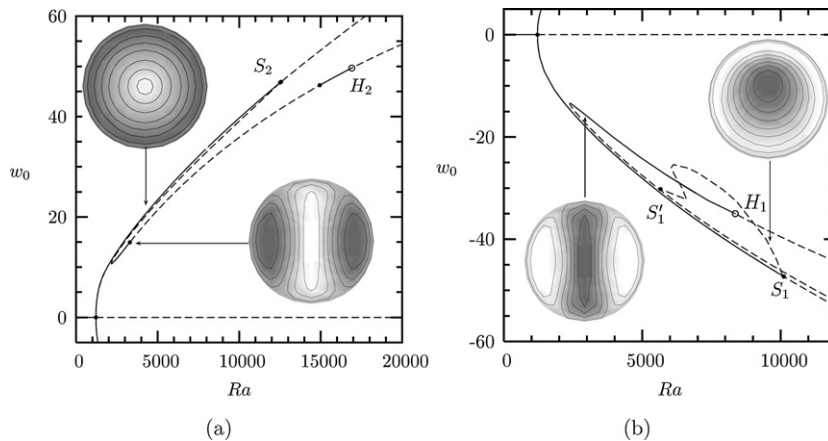
Fig. 4. Zooms on the evolution of the subcritical (a) and supercritical (b) primary branches of the bifurcation diagram shown in Fig. 3.

4. Conclusion

We have numerically computed the thresholds for the onset of the buoyant convection and the nonlinear evolution of this buoyant convection in three-dimensional vertical cylinders heated from below, with a strongly conducting upper surface and adiabatic side walls. Calculations performed for either a rigid upper surface (R-R case) or a non-constrained free surface (R-F case) allowed to emphasize the influence of the constraint at the upper surface. It was shown that the influence of the aspect ratio on the primary thresholds is not much changed between the two cases, except that the thresholds are lower in the case of the free surface and that the transitions between the different modes are delayed to larger aspect ratios. On the contrary, the bifurcation diagrams showing the nonlinear evolution of the flow are much changed between the two cases. Calculations performed in the range of aspect ratios where the onset of convection is to an axisymmetric flow have shown that in the R-R case the two equivalent axisymmetric primary branches bifurcate supercritically to $m = 0/2$ states. In contrast, in the R-F case the two non-equivalent axisymmetric primary branches are connected to the $m = 0/2$ states through subcritical transitions, either directly for one of the axisymmetric branches or through intermediate $m = 0/1$ states for the other branch. Moreover, the subcritical transitions lead to branches with a very strong subcriticity so that in a large range of Rayleigh number values many different solutions co-exist at fixed parameter values.

Acknowledgement

References

[1] R. Touihri, H. Ben Hadid, D. Henry, On the onset of convective instabilities in cylindrical cavities heated from below. I. Pure thermal case, Phys. Fluids 11 (1999) 2078–2088.

[2] E.L. Koschmieder, S.A. Prahl, Surface-tension-driven Bénard convection in small containers, J. Fluid Mech. 215 (1990) 571–583.

[3] P. Cerisier, S. Rahal, H. Azuma, Pattern dynamics of the Bénard–Marangoni instability in a medium aspect ratio container, in: Second International Symposium on Instability and Bifurcations in Fluid Dynamics, in: J. Physics: Conference Series, vol. 64, 2007, p. 012004.

[4] S. Rahal, P. Cerisier, H. Azuma, Bénard–Marangoni convection in a small circular container: Influence of the Biot and Prandtl numbers on pattern dynamics and free surface deformation, Exp. Fluids 43 (2007) 547–554.

[5] A.A. Zaman, R. Narayanan, Interfacial and buoyancy-driven convection – The effect of geometry and comparison with experiments, J. Colloid Interface Sci. 179 (1996) 151–162.

[6] P.C. Dauby, G. Lebon, E. Bouhy, Linear Bénard–Marangoni instability in rigid circular containers, Phys. Rev. E 56 (1997) 520–530.

[7] P. Assemat, A. Bergeon, E. Knobloch, Nonlinear Marangoni convection in circular and elliptical cylinders, Phys. Fluids 19 (2007) 104101.

[8] D. Henry, H. Ben Hadid, Multiple flow transitions in a box heated from the side in low-Prandtl-number fluids, Phys. Rev. E 76 (2007) 016314.